Ultra-High Performance Organic Thermoelectric Generators through Interfacial Doping Gradients

I. Petsagkourakis
Linköping University https://orcid.org/0000-0002-7989-6027
S. Riera-Galindo
Linköping University
Tero-Petri Ruoko
Linköping University
Xenofon Strakosas
Linköping University
Eleni Pavlopoulou
University of Bordeaux https://orcid.org/0000-0002-5291-0132
Xianjie Liu
Linköping University
Slawomir Braun
Linköping University
Nara Kim
Linköping University https://orcid.org/0000-0002-9848-5899
S. Lienemann
Linköping University https://orcid.org/0000-0001-9818-1687
V. Gueskine
Linköping University
Georges Hadziioannou
Universite de Bordeaux
Magnus Berggren
Linköping University https://orcid.org/0000-0001-5154-0291
Mats Fahlman
Linköping University https://orcid.org/0000-0001-9879-3915
Simone Fabiano
Linköping University https://orcid.org/0000-0001-7016-6514
Klas Tybrandt
Linköping University https://orcid.org/0000-0002-9845-446X
Xavier Crispin (✉ xavier.crispin@liu.se)
Linköping University https://orcid.org/0000-0001-8845-6296

Article

Keywords: organic electronic devices, OTEG, organic thermoelectrics, interfacial doping gradients

Posted Date: July 14th, 2020

DOI: https://doi.org/10.21203/rs.3.rs-38396/v1

Abstract

The interfacial energetics are known to play a crucial role in organic electronic devices. However, their effects in organic thermoelectrics remain to be elucidated. In this work we optimize the output power density of an organic thermoelectric generator (OTEG) at ambient atmosphere to record high values, by varying the work function of the metal contacts. We find that the effect is linked to extended gradients of doping states, which are induced by humidity and reside inside the organic layer oriented perpendicular to the metal contacts. The thermovoltage, arising from this contact phenomenon alone, reaches a magnitude similar to that of the Seebeck voltage of the conducting polymer itself, thereby providing a major contribution to the resulting thermoelectric performance. With this work, we put a new emphasis on the importance of the metal-polymer interface in thermoelectrics. The overall output performance can be greatly improved by fine-tuning the interfacial energetics, which then provides an attractive complementing route for enhancing the performance of OTEGs.

Introduction

Thermoelectric devices convert heat flux into electricity, and vice versa. Over the last decade, organic (semi)conductors have attracted major attention from the thermoelectrics community thanks to a series of compelling and unique properties, such as simple processing and manufacturing, mechanical flexibility, high abundance with respect to their atomic elements, as well as electric-to-thermal conductivity ratios (σ/κ) similar to those of conventional inorganic alloys operating at low temperatures (< 200 °C). Various strategies have emerged to increase the Seebeck coefficient (S), power factor (σS^2), and figure of merit ZT (= $\sigma S^2 T/\kappa$) of thermoelectric polymers[1-4]. Today the best-performing organic thermoelectric material comprises positively charged poly(3,4-ethylenedioxythiophene) chains that are charge-compensated with anionic counterions X (PEDOT:X), yielding ZT values in the range 0.25-0.4 at room temperature[5,6]. Although the device geometry has been found to be crucial for measuring the Seebeck coefficient of the materials accurately[7], the reported values without these errors still vary from 15 up to 45 µV/K for PEDOT thin films[1,6,8-12]. Those differences have a significant impact on the thermoelectric power factor and the conversion efficiency, as these quantities are proportional to the square of the Seebeck coefficient.

For an ideal generator, the maximum output power density is found for a load resistance that equals the device (internal) resistance (R_{dev}) of the organic thermoelectric generator (OTEG), and is expressed by $P_{max} = V_{oc}^2/(4\ R_{dev}\ A)$ (Eq. 1), where $V_{oc} = S\,\Delta T$ is the open-circuit voltage (thermovoltage) and A is the device cross-section area. In a simplistic model, one leg of a thermoelectric generator is composed of two metal contacts and the thermoelectric material. In inorganic thermoelectric generators, it is well established that the contact resistance between the metal contact and the thermoelectric material limits the efficiency and power output performance[13,14]. Also, the energetics at the metal-organic semiconductor interface is recognized to play a major role in determining the performance of organic

(opto)electronic devices, such as organic transistors and solar cells,[15] but a similar dependence has never been identified or even investigated for OTEGs.

Here, we report a systematic study on the impact of the metal-organic semiconductor interface energetics on the thermoelectric performance of PEDOT-based OTEGs. We observe that while the Seebeck coefficient of PEDOT films does not vary with the work function of the metal contact when measured in inert and dry atmosphere, *S* systematically increases with increasing the metal work function in humid air. Infrared spectroscopy allows us to identify an interfacial redox reaction occurring between PEDOT and the metal contact[16], which modifies the oxidation level of the polymer in a significant volume of the thin film extending beyond the metal contact interface. Learning from these new insights, we optimize the electrical power output of OTEGs and achieve a record-high value in power density for PEDOT:Toluenesulfonate (PEDOT:Tos)-based OTEGs with Pt as the metal contacts (643.5 μW/cm^2 at room temperature for ΔT= 30°C). We anticipate that our findings of interfacial energetics-thermopower dependence will have a similar impact on the field of organic thermoelectrics as it has had in the context of organic field-effect transistors[17,18] and organic solar cells[19].

Results And Discussion

PEDOT:Poly(4-styrenesulfonate) (PEDOT:PSS) and PEDOT:Tos films (~100 nm thick) were deposited on glass substrates pre-patterned with metal contacts (~100 nm thick). While exposed to ambient air (40 % Relative Humidity (RH), 20 °C), a temperature gradient ΔT is applied between the two electrodes and the open circuit voltage V_{oc} between those two electrodes is measured to estimate the Seebeck coefficient $S = V_{oc}/\Delta T$ (**Fig. S1.1**). The linewidth and inter-distance separation of the metal electrodes were chosen such to minimize the error associated with the estimation of the Seebeck coefficient (**Fig. S1.2**).[7] Five different metals were explored, Al, Ni, Ag, Au, and Pt, covering a range of work function values from 3.7 to 5.2 eV, as measured by ultraviolet photoelectron spectroscopy (**Fig. S2.1**). Note that the presence of humidity does not affect the metal work functions[20], as the latter measured by Kelvin probe for Au, Ag, and Al substrates have similar values both in vacuum and in air (40 %RH) (**Table S2.1**).

We observe that the Seebeck coefficient of PEDOT:Tos [PEDOT:PSS] increases with the work function of the metal contact, from 22.7 μV/K [9.4 μV/K] with Al to 50.5 μV/K [26.3 μV/K] with Pt (**Fig. 1a**). This is a large improvement achieved just by replacing the metal contact and altering the WF. Notably, there is no correlation between the Seebeck coefficients of the metal contacts (open symbols) and the measured Seebeck coefficients (closed symbols). Previous works have reported surprisingly large variations of Seebeck coefficient for both PEDOT:PSS (~10 μV/K with Ag contacts[1,2,9,12] and ~20 μV/K with Au contacts[2,6]) and PEDOT:Tos (40 μV/K with Au contacts[2]). Our results seem to suggest that the large variations in Seebeck coefficient reported in the literature might be due to the different energetics of the chosen metal-organic interface. Furthermore, even for the same type of metal electrode, the effective Seebeck coefficient is also expected to vary slightly, since the effective metal WF – being a surface

property – is affected by the metal surface crystallinity [23], morphology, and also by impurities introduced during metal deposition.

Two metal contacts, set at different temperatures (ΔT = 1 °C around room temperature) and connected to the PEDOT film, constitute a single leg OTEG. The generated electrical power is then measured for various load resistances (**Fig. S2.3**) aiming at finding the maximum output power for $R_{load} = R_{dev}$. The measured maximum output power density P_{max} of the OTEGs based on PEDOT:Tos [PEDOT:PSS] is also increasing with the metal WF, from 0.017 μW/cm^2 [0.003 μW/cm^2] with Al to 0.715 μW/cm^2 [0.105 μW/cm^2] with Pt (**Fig. 1b**). Note that the measured P_{max} (closed symbols) is in rather good agreement with the calculated value based on Eq. 1 (open symbols). As $P \sim \Delta T^2$, the extrapolated power values for ΔT = 30 °C are 643.5 μW/cm^2 for the Pt/PEDOT:Tos/Pt and 94.5 μW/cm^2 for Pt/PEDOT:PSS/Pt (**Fig.1b**). The maximum power density values cannot be explained solely based on the measured Seebeck coefficients. We find that the device resistance of the PEDOT legs also depends on the metal WF. For PEDOT:PSS, R_{dev} varies from 6 kΩ for Al to 0.15 kΩ for Pt (**Fig. 1c**), while for PEDOT:Tos R_{dev} decreases from 0.7 kΩ (Al) to 0.01 kΩ (Pt). Since the channel resistance, measured with the 4-probe method, is constant for the various films (**Fig. 1c**), we attribute the change in R_{dev} to the variation of the contact resistance R_c with the contact metal WF (**Fig. 2c**). In order to provide further evidence on that, we extracted R_c values also for the PEDOT:PSS/Ag contact (6.7 ohm cm) and PEDOT:PSS/Au contact (2.4 ohm cm) and indeed observed a similar dependence for the total device characteristics. Hence, the WF of the metal contact in an OTEG impacts the resulting Seebeck coefficient, the device resistance, and thus its electrical power conversion performance. These findings raise two questions: what is the origin of the interfacial effects and what is the true Seebeck coefficient of PEDOT?

Before designing experiments to answer these two fundamental questions, it is important to remind that the humidity affects the thermoelectric properties of PEDOT:PSS. The reason to this is that the thermodiffusion of ions generates an additional contribution to the Seebeck voltage that has time-dependent and diminishing characteristics.[10,24] In our measurements, carried out at 40 %RH, the Seebeck coefficient is constant over an extended period of time (**Fig. S3.1**), thus indicating the absence of an ionic Seebeck effect. Moreover, there is no additional static voltage as indicated by the fact that the intercept of the thermovoltage *vs* ΔT curve runs through zero (see **Fig. S2.2**). The voltage contribution from the ionic Seebeck effect in PEDOT:PSS is also known to be negligible at relative humidity levels below 40 %[25], and has never been observed in PEDOT:Tos even at elevated humidity levels[9]. With this in mind, we then decided to focus on PEDOT:Tos exposed to 40 %RH in order to investigate the effect of the metal contact WF. Even though PEDOT:Tos does not display any ionic Seebeck effect, due to its low ionic conductivity, computational microscopy[26] supports the presence of water molecules within the film at ambient conditions, which could potentially trigger an interfacial redox reaction.

PEDOT:Tos films were deposited inside a glovebox in an inert and dry atmosphere ([O_2]=3.9 ppm, [H_2O]=3 ppm). The Seebeck coefficients of PEDOT:Tos/Al, PEDOT:Tos/Au, and PEDOT:Tos/Pt were not

dependent on the metal WF, and reach 21±1 μV/K at room temperature, thus matching previously reported values for experiments conducted under the same conditions (**Fig. 2a**)[4]. We believe that this value is the true Seebeck coefficient of the PEDOT:Tos films (i.e., without any contribution introduced by the metal contact). When the samples were exposed to ambient atmosphere (40 %RH at room temperature), the Seebeck coefficient increased from 21 μV/K to 50 μV/K for OTEGs with Pt contacts (**Fig. 2b**). Interestingly, when the samples were re-introduced into the glovebox, the Seebeck coefficient returned back to its original value of 21 μV/K. Next, we identified whether the relative humidity and/or the presence of oxygen were key-parameters to control the Seebeck coefficient. We conducted the thermoelectric measurements in three different atmospheres: dry nitrogen, dry oxygen-nitrogen mixture and humid nitrogen. After transferring the samples to a glovebox filled with dry air (O_2+N_2, -30 °C dew point), we observed a slight increase in the Seebeck coefficient value reaching 25±3 μV/K (**Fig. 2c**). One set of samples was then kept in dry nitrogen atmosphere while it was characterized over an extended period of time. These OTEGs displayed a constant Seebeck coefficient over the entire measurement period. Another set of samples was instead exposed to humid nitrogen and underwent an immediate and rapid increase of the Seebeck coefficient, starting at 25 μV/K and finally reaching 43 μV/K after 20 h of exposure. After 20 h, the exposure to humidity was terminated and dry nitrogen was fed into the chamber. We then observed that the Seebeck coefficient slowly reduced towards its original value of 21 μV/K. The power output recorded from this Au/PEDOT:Tos/Au OTEG leg also displays an evolution that strongly depends on the relative humidity level (**Fig. S2.3**). Consequently, we can then conclude that humidity is a key-parameter to observe the effect of WF on the measured Seebeck coefficient for PEDOT films.

The way S and R_{dev} depend on the WF of the metal contacts pinpoints that the phenomenon responsible for these measured trends relates to the energetics of the metal-polymer interface. Interfacial dipoles are known to form at the conducting polymer-metal electrode interface, and depend on their WFs[15,27-31]. The WF of PEDOT:Tos and PEDOT:PSS is typically 4.5± 0.2 eV eV and 5.0 ± 0.1 eV [32,33], respectively. The equalization of the chemical potential of the electrons at the metal-polymer interface leads to a reorganization of the electronic density (integer charge transfer across the interface) that produces an interfacial dipole[15]. If the Fermi level of the metal is higher [lower] than that of the PEDOT film, PEDOT is oxidized [reduced]. The extension of the interfacial dipole into polymer semiconductor films, measured under vacuum conditions, is typically localized over a few nm.[15] However, when a PEDOT film is exposed to ambient air with 40 %RH, ions from the polymer film can potentially diffuse within the polymer bulk as the interchain interactions are dominated by electrostatic and Van der Waals forces. In other words, PEDOT films are mixed ion-electron conductors with an ionic conductivity that increases exponentially with the relative humidity of the environment[34]. The presence of mobile ions accompanied by the interface charge transfer, driven by electronic chemical potential equilibration between PEDOT and the metal, is expected to form an inhomogeneous oxidation level profile in the PEDOT bulk starting from the interface. This spontaneous reorganization of the electrons and ions due to the Fermi level alignment at the PEDOT-metal interface has not been identified to date. However, it is known that under an external applied bias, generated by two electrodes connecting a PEDOT layer that is also coated with an electrolyte, a potential gradient is created along the PEDOT-electrolyte interface. This then generates an

oxidation profile that results in an electrochromic gradient, a phenomenon that can be observed for instance along the channel of an electrochemical transistor[35].

Vibrational spectroscopy is known to be sensitive to the oxidation level of PEDOT[36-38] and can thus be used to probe the metal-PEDOT interface. To identify the intrinsic vibrational transitions of the polymer, we first measured ATR-FTIR (attenuated total reflectance Fourier transform infrared spectroscopy) of PEDOT:PSS and PEDOT:Tos films on a non-conducting IR-transparent CaF_2 substrate (**Fig. 3b,c** and SI, Section 4). Two important vibrational transitions are the asymmetric C=C stretching mode doublet of the thiophene ring located at 1533 & 1547 cm^{-1} and its symmetric C=C counterpart at 1415 cm^{-1}.[39] Next, infrared reflection absorption spectroscopy (IRAS)[40-42] was used to probe changes in those vibration bands induced by a modification in the oxidation level at the metal-PEDOT interface. From the IRAS spectra for PEDOT:PSS and PEDOT:Tos thin films (thickness ~100 nm) deposited on top of Al, Ag, Au and Pt (**Fig. S.4:1-4**), we focus on the evolution of the frequency of the C=C bonds, see **Figs. 3b-d**. The asymmetric [symmetric] C=C vibration peak maxima of the thiophene unit are located at 1525 cm^{-1} [1417 cm^{-1}] on Al, 1530 cm^{-1} [1415 cm^{-1}] on Ag, 1533 cm^{-1} [1415 cm^{-1}] on Au, and 1535 cm^{-1} [1413 cm^{-1}] on Pt. Compared to the pristine PEDOT film, measured on the insulating CaF_2 substrate, the symmetric peak shift towards lower wavenumbers indicates that PEDOT chains undergo oxidation on the Pt substrate and reduction on the Al substrate.[37] This observation is fully consistent with the expected spontaneous electron transfer occurring between the metal and the PEDOT films. Thus, if the polymer WF is smaller than the metal WF (e.g. platinum), the polymer becomes oxidized at the interface[15]; while if the polymer WF is larger than the metal WF (e.g. aluminum), the polymer gets reduced at the interface compared to the pristine oxidation state of PEDOT. Since the asymmetric peak position of the Au sample is the same as with the pristine PEDOT:PSS, there is no apparent interfacial redox reaction. However, there is an interfacial redox reaction between PEDOT:Tos and Au, as the asymmetric peak of the pristine PEDOT:Tos is lower than that of PEDOT:Tos/Au, which is likely due to the lower WF of PEDOT:Tos compared to PEDOT:PSS.

In IRAS, the incident infrared light is reflected at grazing incidence by the metal surface so that the absorbed wavelengths correspond to transitions in the vibrational modes of PEDOT at the metal interface, as well as in the bulk of the thin film. Tuning the thickness of the PEDOT film provides us with a probe to study the volumetric extension of this redox phenomenon. When there is no interfacial redox reaction, as identified for the PEDOT:PSS/Au system, the peak positions remain constant while increasing the polymer thickness from 100 to 800 nm, although we do observe a slight trend in the peak ratios of the asymmetric C=C doublet. In contrast, the $C=C_{asym}$ peak of PEDOT:PSS on Al [Ag] varies with the thickness from 1525 cm^{-1} [1531 cm^{-1}] for a 100 nm thick film to 1531 cm^{-1} [1533 cm^{-1}] for a 800 nm thick film (**Fig 3e-h**, **Fig. S4.5**). This supports the formation of an oxidation level profile within the PEDOT film that extends from the metal-interface into the polymer bulk, reaching up to several hundreds of nanometers of thickness.

Electrochemical doping/dedoping of PEDOT thin films is known to alter its crystalline structure[43]. We studied changes in morphology, induced by the oxidation level profile triggered by the redox interfacial chemistry, by using grazing incidence wide angle X-ray scattering (GIWAXS). As the metals themselves have a strong scattering contribution, we deposited a very thin layer (10 nm) of Au and Al on Si (with native oxide) followed by the deposition of the PEDOT films on top. 2D GIWAXS scattering patterns (**Fig. S5.1**) were recorded and a background (Si+metal) subtraction was carried out. This allowed us to decouple the pure PEDOT contribution (**Fig. 4 inset)**, which was also integrated to obtain the 1D scattering patterns. The scattering features observed for both PEDOT:Tos and PEDOT:PSS agree well with those previously reported in literature[43,44]. Interestingly, a higher degree of order (i.e. a higher integrated (100) peak intensity) is observed for PEDOT in contact with Au as compared to Al, which is consistent with the higher oxidation level of PEDOT:Tos on Au[43].

The interfacial redox chemistry found at the interface between the metal contact and the PEDOT film in OTEG legs is promoted by the WF differences of the metal and the polymer, along with the kinetics of ions that are boosted by the presence of humidity. In order to better understand the full impact and opportunity of the WFs in OTEGs, we propose that the interfacial energetics should be taken into the account while characterizing and optimizing OTEGs in the future. We believe that the description of the electric potential profile along the metal-polymer-metal OTEG leg, submitted to a temperature gradient, should include the drop in Seebeck potential within the PEDOT (S_m=dV/dT) film, as well as the two dissimilar interfacial potential drops located at the hot ($V_{int}(T_H)$) and cold sides ($V_{int}(T_c)$). With such a description (**Fig. S6.1**), the temperature dependence of the interface potential drop $V_{int}(T) = f(T)$ dictates if the measured Seebeck coefficient is larger or smaller than the true Seebeck coefficient of the polymer, through $S_{meas} = S_m + [V_{int}(T_c) - V_{int}(T_H)]/dT$. Beyond the scope of this article, more efforts should also be devoted to investigate the details of the origin and temperature evolution of those interfacial phenomena in order to reach a quantitative model of the effective Seebeck coefficient and generated power in OTEGs. Note also that the temperature dependence of those interfacial potentials also offer yet another degree of freedom to optimize OTEGs. Recently, dissimilar metallic contacts have suggested a modification of the Seebeck coefficient by surface polarization effects[45]. In our case, OTEGs based on different metal contacts, as in the case with Pt/PEDOT:PSS/Ag (S_{meas}= 29.5 µW/K) and Pt/PEDOT:Tos/Ag (S_{meas}= 52.5 µW/K) devices, exhibit higher effective Seebeck coefficient (see **Fig. S7.1**) than with same metals (S_{meas}= 50.5 µV/K).

Finally, we highlight the importance of the interfacial energetics on the OTEG performance, by comparing the remarkably high value of P_{max} obtained with Pt contacts with values found in the literature (**Fig.5**). Since our devices are based on a single element, as a proof of concept for the phenomenon, we expect that even higher power output could be achieved through proper device fabrication (*i.e.*, by optimizing the number and dimensions of the thermoelectric elements). It is evident from **Fig.5** that interfacial energetics can severely enhance the output power of OTEGs, we manage to significantly enhance the thermoelectric performance and reach a record-high OTEG output power. Our study thus opens up a new pathway towards the optimization of organic thermoelectric technology.

Moreover, our discovery of a doping gradient within the polymer bulk, extending away from the various metal contacts, is of direct relevance for the field of organic electronics in general, as metal-conducting polymer interface is a fundamental elementin many devices. A better understanding of these polymer-metal interfaces will impact the performance and efficiencies of several devices, from solar cells to supercapacitors and batteries, to organic electrochemical transistors and more.

Methods

Details on all processes for material and device fabrication are provided in the Supplementary Information (**Section S9**). For all metals the deposition rates were 1 Å per second. Pt was electrodeposited on Au electrodes following the work of Strakosas *et al*[46]. The PEDOT:PSS dispersions with 5 v-% DMSO[6] were deposited on the films through spin coating. PEDOT:Tos was polymerized with in-situ wet chemical oxidative polymerization with a procedure that is reported elsewhere[32]. The 4-point probe sheet resistance was measured with a Keithley 4200. The thermoelectric measurements were conducted with a in-lab setup (**Fig. S2.1**) and details on the device geometry are provided in the Supporting Information. The contact resistances were extracted with the transmission line method following a previous report[47]. The device geometry is presented in **Fig. S8.1**. Details on the IRAS, UPS, GIWAXS and Kelvin Probe characterizations are provided in the Supporting Information.

Declarations

Acknowledgements

The authors acknowledges Prof. I. Zozoulenko, Prof. M. P. Jonsson, Prof. E. Glowacki, Dr. M. Linares and Dr. H. Sun of LOE, Linköping University, Dr. Y. Xia at IFM, Linköping University, and Dr. S.M. Gali, University of Mons, for fruitful discussions. We also acknowledge Mr. L. Gustavsson, Mr. M. Karami Rad, and Mr. T. Karlsson for their technical assistance in realizing the environmental glovebox experiments and their outstanding support in technical issues with our characterization equipment, and Dr. F. N. Ajjan Godoy for assistance in drawing of chemical molecules. This work was financially supported by the Knut and Alice Wallenberg Foundation (Tail of the sun), the EU project (ESR 955837_HORATES), the Swedish Research Council (2016–06146, 2016–03979), ÅForsk (18–313), the Finnish Foundation for Technology Promotion, Swedish Foundation for Strategic Research and the Swedish Government Strategic Research Area in Materials Science on Advanced Functional Materials at Linköping University (Faculty Grant SFO-Mat-LiU No. 2009 – 00971).

References

1. Petsagkourakis, I. *et al.* Thermoelectric materials and applications for energy harvesting power generation. *Science and technology of advanced materials* **19**, 836–862 (2018).

2. Petsagkourakis, I., Kim, N., Tybrandt, K., Zozoulenko, I. & Crispin, X. Poly(3,4-ethylenedioxythiophene): Chemical Synthesis, Transport Properties, and Thermoelectric Devices. *Advanced Electronic Materials* **5**, 1800918, doi:10.1002/aelm.201800918 (2019).
3. Zaia, E. W., Gordon, M. P., Yuan, P. & Urban, J. J. Progress and Perspective: Soft Thermoelectric Materials for Wearable and Internet-of-Things Applications. *Advanced Electronic Materials* **5**, doi:10.1002/aelm.201800823 (2019).
4. Weathers, A. *et al.* Significant electronic thermal transport in the conducting polymer poly(3,4-ethylenedioxythiophene). *Adv Mater* **27**, 2101–2106, doi:10.1002/adma.201404738 (2015).
5. Bubnova, O. *et al.* Optimization of the thermoelectric figure of merit in the conducting polymer poly(3,4-ethylenedioxythiophene). *Nat Mater* **10**, 429–433, doi:10.1038/nmat3012 (2011).
6. Kim, G. H., Shao, L., Zhang, K. & Pipe, K. P. Engineered doping of organic semiconductors for enhanced thermoelectric efficiency. *Nat Mater* **12**, 719–723, doi:10.1038/nmat3635 (2013).
7. Reenen, S. v. & Kemerink, M. Correcting for contact geometry in Seebeck coefficient measurements of thin film devices. *Organic Electronics* **15**, 2250–2255, doi:10.1016/j.orgel.2014.06.018 (2014).
8. Anno, H., Nishinaka, T., Hokazono, M., Oshima, N. & Toshima, N. Thermoelectric Power-Generation Characteristics of PEDOT:PSS Thin-Film Devices with Different Thicknesses on Polyimide Substrates. *Journal of Electronic Materials* **44**, 2105–2112, doi:10.1007/s11664-015-3668-x (2015).
9. Linseis, V. *et al.* Complete Thermoelectric Characterization of PEDOT:PSS Thin Films with a Novel ZT Test Chip Platform. *physica status solidi (a)* **215**, doi:10.1002/pssa.201700930 (2018).
10. Kim, G.-H., Kim, J. & Pipe, K. P. Humidity-dependent thermoelectric properties of poly(3,4-ethylenedioxythiophene):poly(styrene sulfonate). *Applied Physics Letters* **108**, doi:10.1063/1.4942598 (2016).
11. Wijeratne, K. *et al.* Bulk electronic transport impacts on electron transfer at conducting polymer electrode–electrolyte interfaces. *Proceedings of the National Academy of Sciences* **115**, 11899–11904 (2018).
12. Andrei, V. *et al.* Size Dependence of Electrical Conductivity and Thermoelectric Enhancements in Spin-Coated PEDOT:PSS Single and Multiple Layers. *Advanced Electronic Materials* **3**, doi:10.1002/aelm.201600473 (2017).
13. Bjørk, R. An Analytical Model for the Influence of Contact Resistanceon Thermoelectric Efficiency. *Journal of Electronic Materials* **45**, 1301–1308, doi:10.1007/s11664-015-4014-z (2016).
14. Bjørk, R. The Universal Influence of Contact Resistance on the Efficiency of a Thermoelectric Generator. *Journal of Electronic Materials* **44**, 2869–2876, doi:10.1007/s11664-015-3731-7 (2015).
15. Fahlman, M. *et al.* Interfaces in organic electronics. *Nature Reviews Materials* **4**, 627–650 (2019).
16. Sehati, P. *et al.* Energy-Level Alignment at Metal–Organic and Organic–Organic Interfaces in Bulk-Heterojunction Solar Cells. *IEEE Journal of Selected Topics in Quantum Electronics* **16**, 1718–1724, doi:10.1109/jstqe.2010.2042684 (2010).

17. Fabiano, S., Braun, S., Fahlman, M., Crispin, X. & Berggren, M. Effect of Gate Electrode Work-Function on Source Charge Injection in Electrolyte-Gated Organic Field-Effect Transistors. *Advanced Functional Materials* **24**, 695–700, doi:10.1002/adfm.201302070 (2014).
18. Ablat, A. *et al.* Role of Oxide/Metal Bilayer Electrodes in Solution Processed Organic Field Effect Transistors. *Sci Rep* **9**, 6685, doi:10.1038/s41598-019-43237-z (2019).
19. Almosni, S. *et al.* Material challenges for solar cells in the twenty-first century: directions in emerging technologies. *Sci Technol Adv Mater* **19**, 336–369, doi:10.1080/14686996.2018.1433439 (2018).
20. Carrasco, J., Hodgson, A. & Michaelides, A. A molecular perspective of water at metal interfaces. *Nature Materials* **11**, 667–674, doi:10.1038/nmat3354 (2012).
21. Moore, J. P. & Graves, R. S. Absolute Seebeck coefficient of platinum from 80 to 340 K and the thermal and electrical conductivities of lead from 80 to 400 K. *Journal of Applied Physics* **44**, 1174–1178, doi:10.1063/1.1662324 (1973).
22. Shakouri, A. & Suquan, L. in *Eighteenth International Conference on Thermoelectrics. Proceedings, ICT'99 (Cat. No.99TH8407).* 402–406.
23. Fall, C. J., Binggeli, N. & Baldereschi, A. Work functions at facet edges. *Phys Rev Lett* **88**, 156802, doi:10.1103/PhysRevLett.88.156802 (2002).
24. Wang, H., Ail, U., Gabrielsson, R., Berggren, M. & Crispin, X. Ionic Seebeck Effect in Conducting Polymers. *Advanced Energy Materials* **5**, doi:10.1002/aenm.201500044 (2015).
25. Kyaw, A. K. K., Wong, G. D. H., Yemata, T. A. & Xu, J. Effective ionic Seebeck component suppression in mixed ion-electron conductor via chemical treatment. *Organic Electronics* **69**, 7–12, doi:https://doi.org/10.1016/j.orgel.2019.02.014 (2019).
26. Franco-Gonzalez, J. F. & Zozoulenko, I. V. Molecular Dynamics Study of Morphology of Doped PEDOT: From Solution to Dry Phase. *J Phys Chem B* **121**, 4299–4307, doi:10.1021/acs.jpcb.7b01510 (2017).
27. Veenstra, S. C. *et al.* Energy level alignment at the conjugated phenylenevinylene oligomer/metal interface. *Applied Physics Letters* **76**, 2253–2255, doi:10.1063/1.126312 (2000).
28. Jönsson, S. K. M., Salaneck, W. R. & Fahlman, M. Spectroscopy of ethylenedioxythiophene-derived systems: from gas phase to surfaces and interfaces found in organic electronics. *Journal of Electron Spectroscopy and Related Phenomena* **137–140**, 805–809, doi:10.1016/j.elspec.2004.02.120 (2004).
29. Zojer, E., Taucher, T. C. & Hofmann, O. T. The Impact of Dipolar Layers on the Electronic Properties of Organic/Inorganic Hybrid Interfaces. *Advanced Materials Interfaces* **6**, 1900581, doi:10.1002/admi.201900581 (2019).
30. Bao, Q., Braun, S., Wang, C., Liu, X. & Fahlman, M. Interfaces of (Ultra)thin Polymer Films in Organic Electronics. *Advanced Materials Interfaces* **6**, 1800897, doi:10.1002/admi.201800897 (2019).
31. Yang, J.-P., Bussolotti, F., Kera, S. & Ueno, N. Origin and role of gap states in organic semiconductor studied by UPS: as the nature of organic molecular crystals. *Journal of Physics D: Applied Physics* **50**, 423002, doi:10.1088/1361-6463/aa840f (2017).

32. Petsagkourakis, I. *et al.* Correlating the Seebeck coefficient of thermoelectric polymer thin films to their charge transport mechanism. *Organic Electronics* **52**, 335–341, doi:https://doi.org/10.1016/j.orgel.2017.11.018 (2018).
33. Håkansson, A. *et al.* Effect of (3-glycidyloxypropyl)trimethoxysilane (GOPS) on the electrical properties of PEDOT:PSS films. *Journal of Polymer Science Part B: Polymer Physics* **55**, 814–820, doi:10.1002/polb.24331 (2017).
34. Wang, H., Ail, U., Gabrielsson, R., Berggren, M. & Crispin, X. Ionic Seebeck effect in conducting polymers. *Advanced Energy Materials* **5**, 1500044 (2015).
35. Inal, S., Malliaras, G. G. & Rivnay, J. Optical study of electrochromic moving fronts for the investigation of ion transport in conducting polymers. *Journal of Materials Chemistry C* **4**, 3942–3947, doi:10.1039/C5TC04354A (2016).
36. Mitraka, E. *et al.* Oxygen-induced doping on reduced PEDOT. *J Mater Chem A Mater* **5**, 4404–4412, doi:10.1039/c6ta10521a (2017).
37. Khan, Z. U. *et al.* Acido-basic control of the thermoelectric properties of poly(3,4-ethylenedioxythiophene)tosylate (PEDOT-Tos) thin films. *J Mater Chem C Mater* **3**, 10616–10623, doi:10.1039/c5tc01952d (2015).
38. Lee, Y. Y. *et al.* Growth Mechanism of Strain-Dependent Morphological Change in PEDOT:PSS Films. *Sci Rep* **6**, 25332, doi:10.1038/srep25332 (2016).
39. Chiu, W. W., Travaš-Sejdić, J., Cooney, R. P. & Bowmaker, G. A. Spectroscopic and conductivity studies of doping in chemically synthesized poly(3,4-ethylenedioxythiophene). *Synthetic Metals* **155**, 80–88, doi:https://doi.org/10.1016/j.synthmet.2005.06.012 (2005).
40. Golden, W. G., Saperstein, D. D., Severson, M. W. & Overend, J. Infrared reflection-absorption spectroscopy of surface species: a comparison of Fourier transform and dispersion methods. *The Journal of Physical Chemistry* **88**, 574–580, doi:10.1021/j150647a049 (1984).
41. Rabolt, J., Jurich, M. & Swalen, J. Infrared reflection-absorption studies of thin films at grazing incidence. *Applied Spectroscopy* **39**, 269–272 (1985).
42. Tolstoy, V. P., Chernyshova, I. & Skryshevsky, V. A. *Handbook of infrared spectroscopy of ultrathin films*. (John Wiley & Sons, 2003).
43. Aasmundtveit, K. E. *et al.* Structural aspects of electrochemical doping and dedoping of poly(3,4-ethylenedioxythiophene). *Synthetic Metals* **113**, 93–97, doi:https://doi.org/10.1016/S0379-6779(00)00181-8 (2000).
44. Bubnova, O. *et al.* Semi-metallic polymers. *Nature Materials* **13**, 190–194, doi:10.1038/nmat3824 (2013).
45. Peng, L. & Liu, Z. Enhancing thermoelectric properties by using a surface polarization effect based on PEDOT:PSS thin films. *Journal of Materials Chemistry C* **7**, 6120–6128, doi:10.1039/c8tc06616g (2019).
46. Strakosas, X. *et al.* Catalytically enhanced organic transistors for in vitro toxicology monitoring through hydrogel entrapment of enzymes. *Journal of Applied Polymer Science* **134**,

doi:10.1002/app.44483 (2017).

47. Kirihara, K., Wei, Q., Mukaida, M. & Ishida, T. Reduction of specific contact resistance between the conducting polymer PEDOT:PSS and a metal electrode by addition of a second solvent during film formation and a post-surface treatment. *Synthetic Metals* **246**, 289–296, doi:https://doi.org/10.1016/j.synthmet.2018.11.005 (2018).

Figures

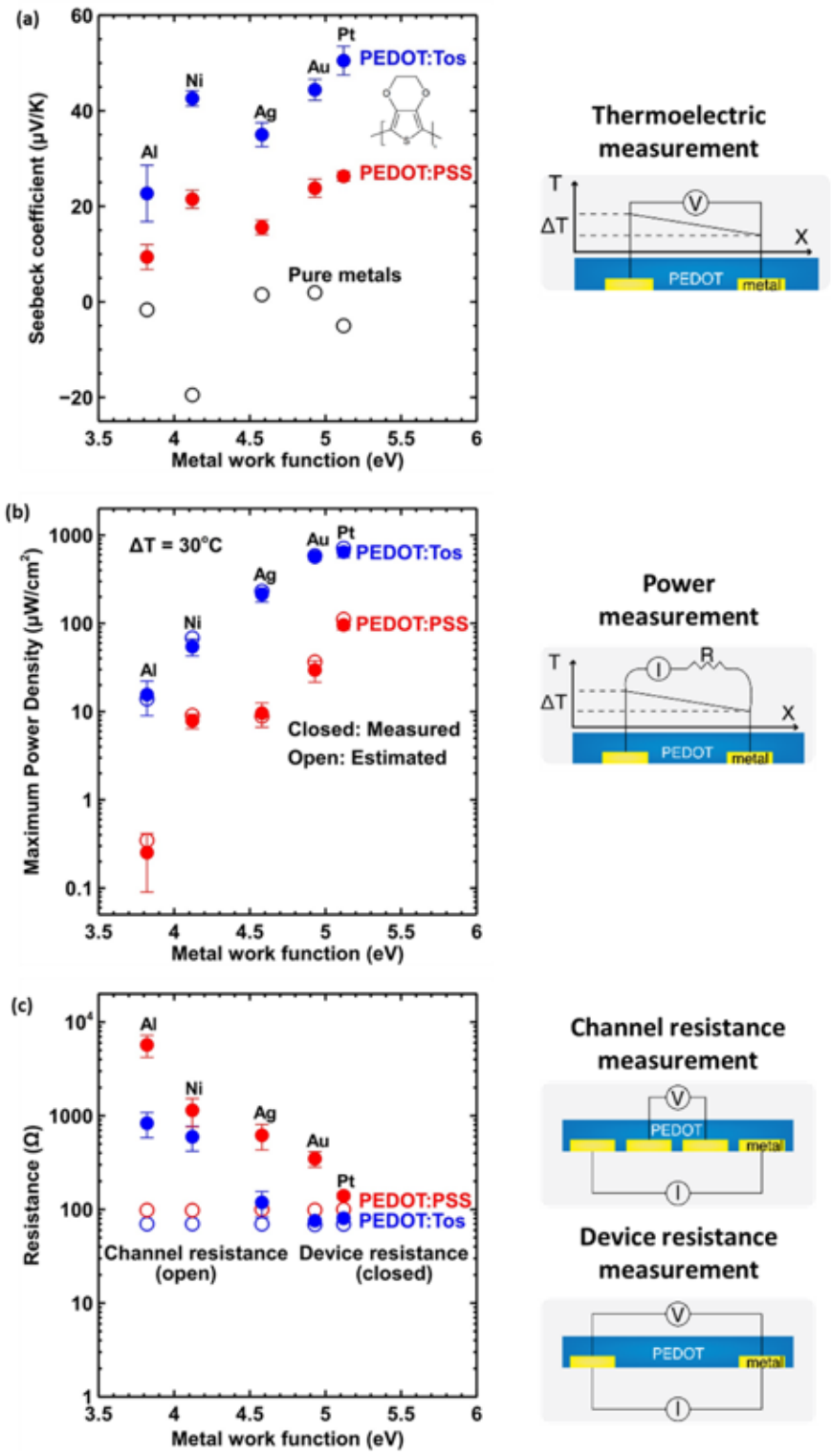

Figure 1

Thermoelectric and electrical characterizations (a) The Seebeck coefficient plotted against the work function of the metal contact for PEDOT:PSS and PEDOT:Tos films (closed) and the pure metals (open)21,22. (b) The respective maximum power density for those devices with the comparison between the estimated value (closed) and the measured value (open) at ΔT = 30 °C. (c) The device (internal) resistance (closed) versus the metal work function for PEDOT films and the respective channel resistance

(open), as measured with a 4-point probe measurement. Schematics of the measurements are provided on the right side of the plots.

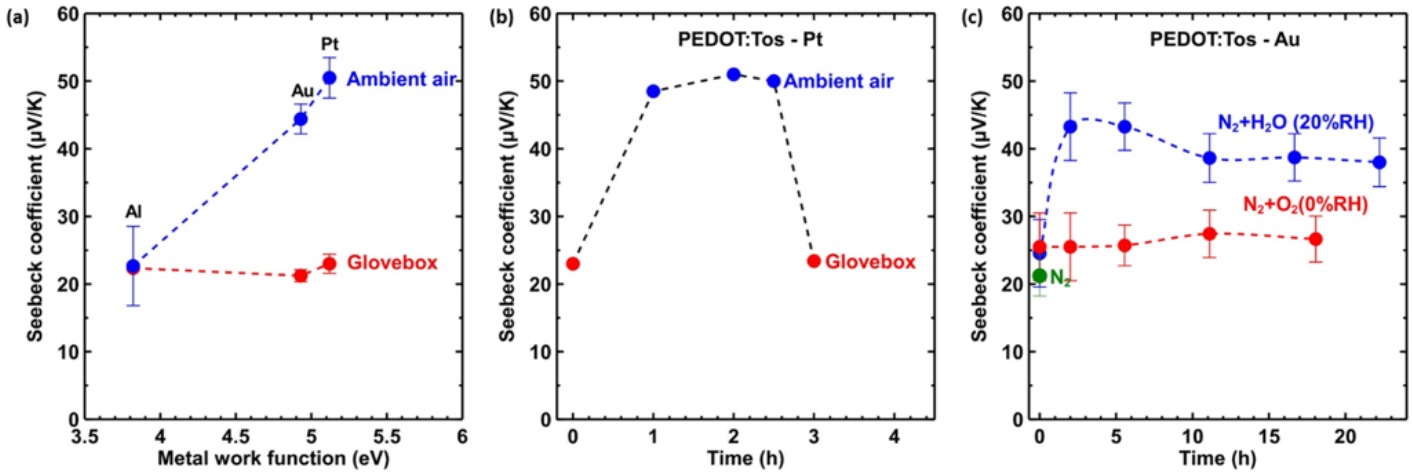

Figure 2

Thermoelectric characterization under different atmospheric conditions: (a) The Seebeck coefficient of PEDOT:Tos fabricated and measured inside the glovebox, in comparison with ones that were fabricated and measured in air. (b) The Seebeck coefficient of PEDOT:Tos/Pt fabricated and measured inside the glovebox, depicted as it is exposed to air and returned back to the glovebox. (c) The Seebeck coefficient of PEDOT:Tos/Au under various atmospheric conditions.

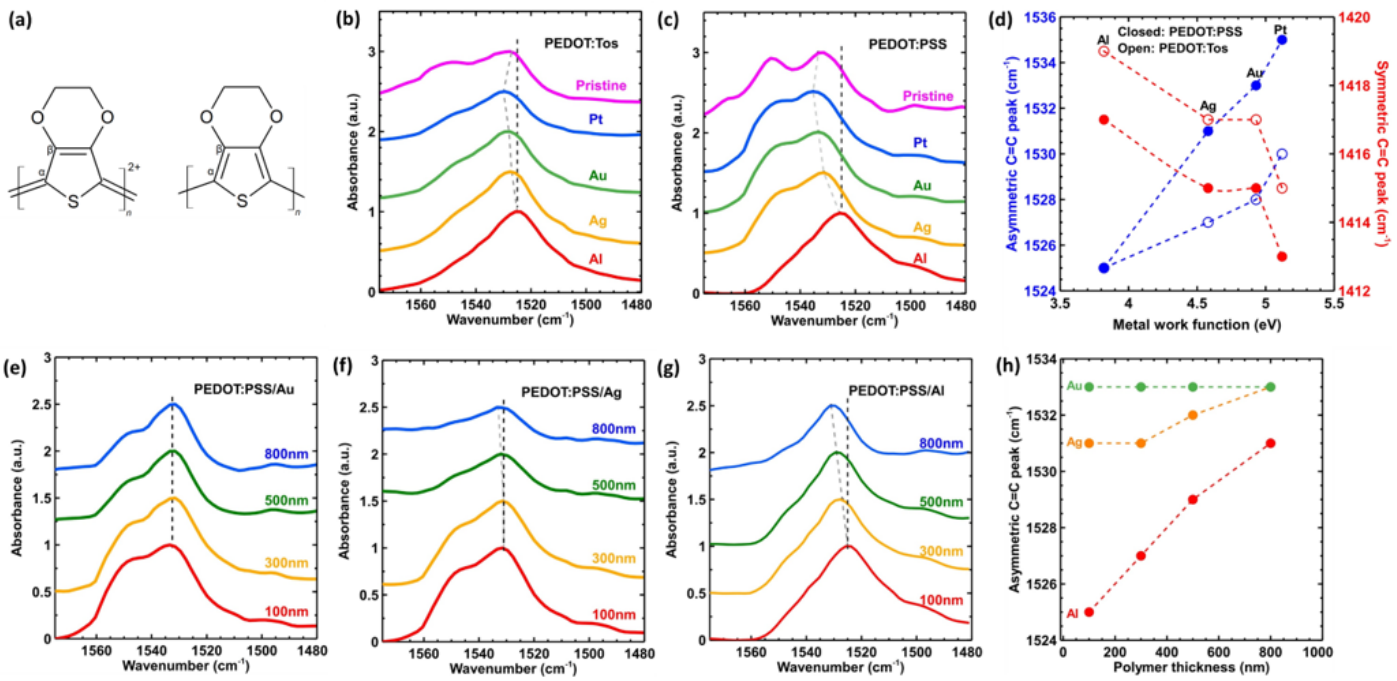

Figure 3

Spectroscopic characterization of the polymer-metal interface (a) Schematic representation of PEDOT in the quinoid (doped) (left) and benzoid (undoped) (right) forms. (b) IRAS absorption spectra of PEDOT:Tos and (c) PEDOT:PSS films (~100 nm thick) on various metal substrates: Al, Ag, Au, and Pt. ATR-FTIR spectra if pristine PEDOT was measured on CaF2. We show here the evolution of the assymetric C=C peak for those systems (dashed line), while the full spectra are provided in the supplementary information. (d) Evolution of the asymmetric and symmetric C=C band maxima of the thiophene ring for PEDOT:PSS (closed) and PEDOT:Tos (open) on the various metals. (e-g) IRAS spectra of PEDOT:PSS of varying thicknesses on (e) Au, (f) Ag, and (g) Al. We show here the evolution of the assymetric C=C peak for those systems (dashed line, full spectra in supplementary information). (h) Evolution of the asymmetric and symmetric C=C band maxima of the thiophene ring for PEDOT:PSS of various thicknesses on Au, Ag and Al.

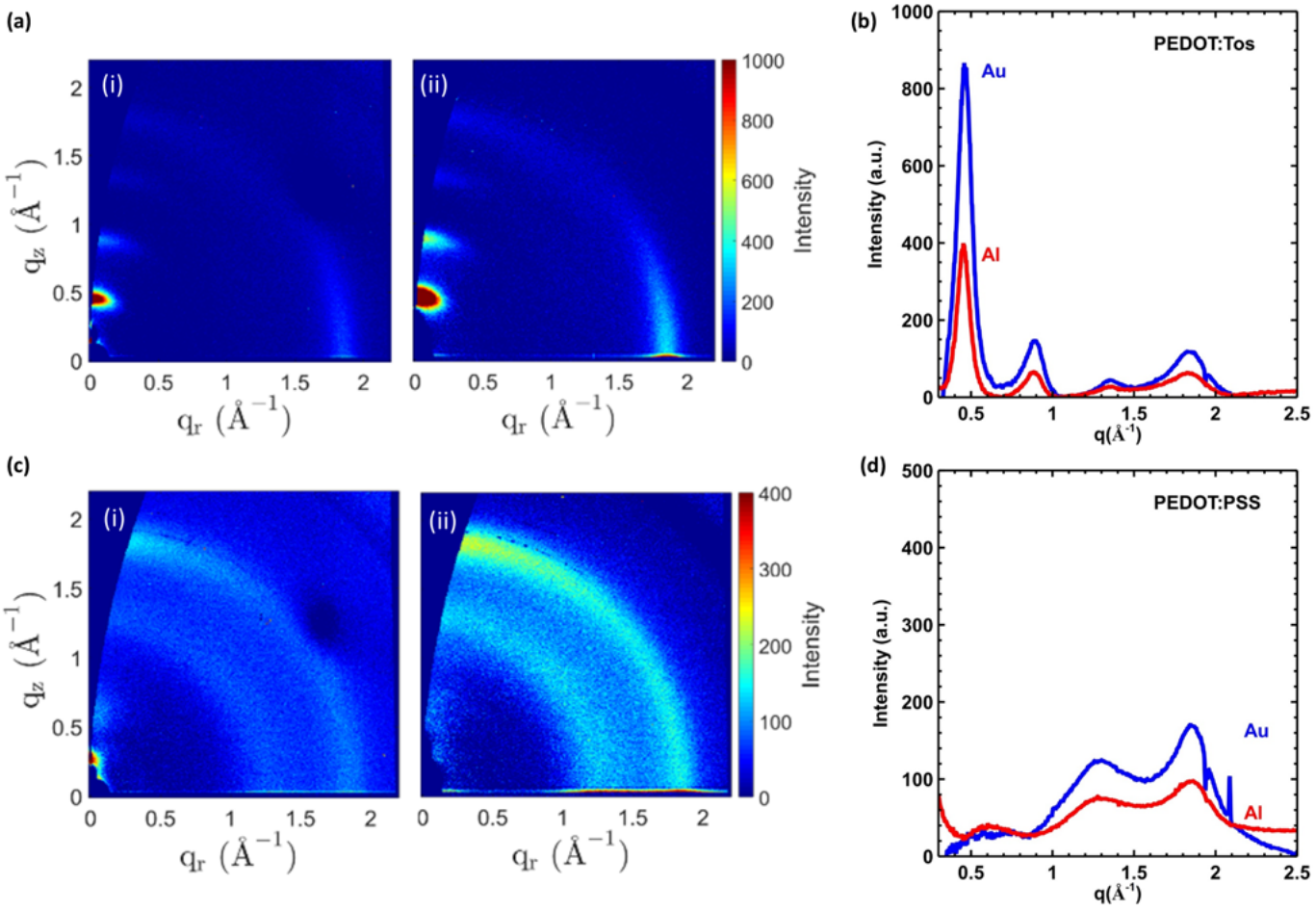

Figure 4

Morphological characterization of the polymer-metal layers (a) The 2D background subtracted scattering images for PEDOT:Tos on Al (i) and Au(ii). (b) The 1-D scattering patterns for PEDOT:Tos on Au and Al. (c) The 2D background subtracted scattering images for PEDOT:PSS on Al (i) and Au(ii). (d) The respective 1-D scattering patterns for PEDOT:PSS on Au and Al.

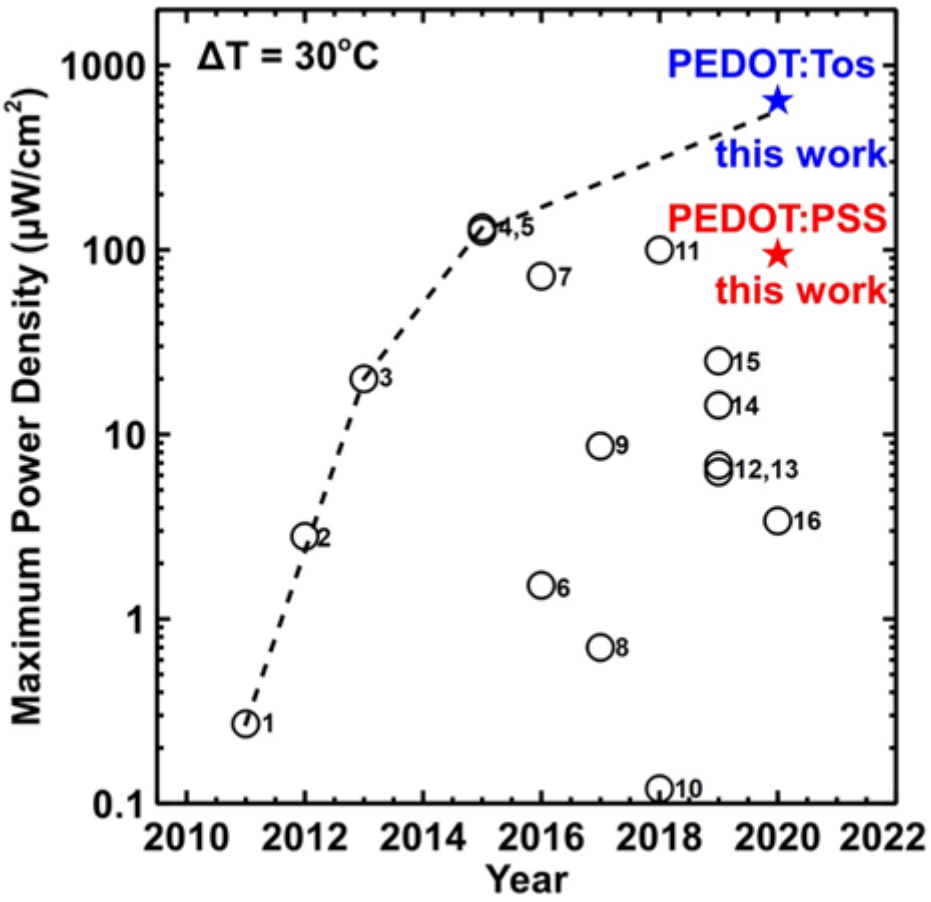

Figure 5

The state-of-the-art: Comparison of the Maximum Power Density for ΔT = 30 °C for our systems (stars) and other works in the literature (open). In the supplementary information we provide details on the values obtained from literature. Given that power density follows a parabolic law of P~ ΔT2 , we converted the various values into power densities (following the dimensions and details provided) and then into the range of ΔT = 30 °C; we provide all the information on the conversion in Table S7.1.

Supplementary Files

This is a list of supplementary files associated with this preprint. Click to download.

- SUPINFOmetalmanuscriptversion20200624.docx